THE ASTROPHYSICAL JOURNAL, 434:67–81, 1994 October 10

HIGH-RESOLUTION OPTICAL AND UV OBSERVATIONS OF THE CENTERS OF NGC 1316 AND NGC 3998 WITH THE *HUBBLE SPACE TELESCOPE*[1]

G. FABBIANO, C. FASSNACHT,[2] AND G. TRINCHIERI[3]
Harvard-Smithsonian Center for Astrophysics, 60 Garden Street, Cambridge, MA 02138
Received 1993 August 2; accepted 1994 April 21

ABSTRACT

B and UV high-resolution images obtained with the *HST* FOC reveal centrally increasing surface brightness and UV-bright point sources at the nuclei of the early-type galaxies NGC 1316 and NGC 3998. Model fitting of the surface brightness distribution does not exclude a central flattening, which could however be the result of extinction and/or of improper evaluation of the point-source component. The present data, while not requiring the presence of central massive black holes in these two galaxies, make them possible candidates. Follow-up work is needed to study this point further. The presence of unresolved nuclei gives model-dependent support to this quest, if these sources are due to small AGN. These UV-bright sources could belong to the low-luminosity end of active nuclear emission.

Subject headings: galaxies: active — galaxies: individual (NGC 1316, NGC 3998) — galaxies: nuclei — ultraviolet: galaxies

1. INTRODUCTION

The study of the light distribution in the central regions of elliptical galaxies can give us important clues on their formation and growth, and on the presence of a large central mass concentration. These studies, however, have typically been hampered by the effect of seeing (e.g., Schweizer 1981). *HST*, even with its aberrated optics, gives us a direct way to infer the distribution of light in the central regions of galaxies, down to radii well below 1″.

NGC 1316 and NGC 3998 are two early-type galaxies (S0), which exhibit nuclear activity. NGC 1316 is a nearby radio galaxy (Fornax A), with a core-jet-lobes structure (Geldzahler & Fomalont 1984). NGC 3998 hosts a compact radio source (see Fabbiano, Gioia, & Trinchieri 1989). The central regions of both galaxies have low-ionization emission-line spectra (Baum, Heckman, & Van Breugel 1992; Heckman, Balick, & Crane 1980; Keel 1983), and there is evidence for circumnuclear emission-line disks (Ford et al. 1986; M. Frank 1993, private communication; F. Bertola 1993, private communication). NGC 3998 has also been studied in the IR as part of a sample of LINERs (Willner et al. 1985); UV observations with *IUE* (Reichert et al. 1992) suggest the presence of a nuclear point source, with strong broad Mg II (2800 Å) emission. Both galaxies have been observed in X-rays with *Einstein* (e.g., Fabbiano, Kim, & Trinchieri 1992; Kim, Fabbiano, & Trinchieri 1992). The ∼5″ resolution observation of NGC 1316 shows that the X-ray emission is extended, and there is no evidence of a strong nuclear point source. The X-ray emission of NGC 3998 is unresolved; however, this galaxy was observed only at low spatial resolution (∼40″) with *Einstein*. A study of the optical surface brightness of the central regions of NGC 1316 (Schweizer 1981) led to the detection of a small bright core, and to the suggestion of a heavily absorbed nucleus.

The presence of nuclear radio sources in NGC 1316 and NGC 3998 makes them likely candidates for hosting central massive black holes. Accretion onto massive black holes has been invoked as the energy source of quasars and active galactic nuclei (Rees 1984). Based on a correlation between the core radio luminosity of quasars and bright 3CR galaxies, and their X-ray luminosity (Fabbiano et al. 1984), one can predict X-ray luminosities for the active nuclei. These estimates are below the detected *Einstein* luminosities of these galaxies which are likely to be dominated by an extended gaseous component (Fabbiano, Gioia, & Trinchieri 1989). Predictions on the X-ray emission of an active nucleus can be turned into limits on the mass of a central black hole, following Fabian & Canizares (1988), who consider accretion from the hot ISM as the fueling mechanism for the nuclear black hole. For NGC 1316 and NGC 3998 these limits suggest black hole masses between 10^4 and 10^8 $M_\odot$ (see Fabbiano et al. 1989).

In this paper we report the results of high-resolution observations of NGC 1316 and NGC 3998 with the *HST* FOC in the optical and UV. There were two motivations for these observations: we wanted to find or set limits on the luminosity of nuclear point sources, which could be the optical-UV counterparts of the radio-emitting nucleus; and we wanted to study the surface brightness distributions in the inner regions of these galaxies to seek the dynamical signature of a central mass concentration.

The presence of a large central mass concentration would have visible effects on the radial distributions of both stellar surface brightness and velocity dispersion, which should be increasing at smaller radii. Although a number of ellipticals can be fitted with King profiles (e.g., King 1978), even before space observations it was known that some galaxies presented deviations from a flat-core King distribution in their inner regions (see Lauer 1985). Direct evidence of massive black holes has been sought with high-resolution observations of the inner regions of nearby galaxies both from the ground (e.g., Young et al. 1978; Sargent et al. 1978; Dressler 1980; Dressler & Richstone 1990; Kormendy 1992; Kormendy 1988a, b; Richstone, Bower, & Dressler 1990) and more recently and effectively with *HST*. Perhaps the best studied example is M87,

[1] Based on observations with the NASA/ESA *Hubble Space Telescope*, obtained at the Space Telescope Science Institute, which is operated by AURA, Inc. under NASA contract NAS5-26555.

[2] Presently at Caltech, Pasadena, CA 91125.

[3] Also Osservatorio Astronomico di Brera, Via Brera 28, Milano 20121, Italy.

TABLE 1

OBSERVATION LOG (FOC; F96 MODE)

Filters[a]	λ_0[b] (Å)	$\Delta\lambda$ (Å)	Start Time[c]	Stop Time[c]	Exposure Time (s)
NGC 1316: Field Center (J2000): R.A. $03^h22^m41^s.73$; decl. $-37°12'29''.78$					
F480LP F2ND, F1ND	5080	722	48654.46802 (1992 Feb 1, 18:13:57[d])	48654.47329 (1992 Feb 1, 18:21:32[d])	455.75
F175W	1720	678	48654.52714 (1992 Feb 2, 19:39:05)	48654.55070 (1992 Feb 2, 20:13:01)	1644.13
NGC 3998: Field Center (J2000): R.A. $11^h57^m56^s.09$; decl. $+55°27'12''.76$					
F480LP F2ND, F1ND	5080	722	48655.49150 (1992 Feb 2, 18:47:46)	48655.49677 (1992 Feb 2, 18:55:21)	455.75
F342W F1ND	3400	704	48655.50075 (1992 Feb 2, 19:01:05)	48655.50348 (1992 Feb 2, 19:05:01)	235.75
F175W	1720	678	48655.55607 (1992 Feb 2, 20:20:45)	48655.55828 (1992 Feb 2, 20:23:55)	191.38

[a] F1ND and F2ND are neutral density filters with attenuations of 70% and 90%, respectively.
[b] Peak wavelength.
[c] Modified Julian Date.
[d] All times in EST.

where the discovery of a central power-law component of the light distribution, coupled with a centrally rising stellar velocity dispersion, led to the debated suggestion of the presence of a central massive black hole (Young et al. 1978; Sargent et al. 1978; Dressler & Richstone 1990). *HST* observations of M87 have confirmed the presence of a centrally rising light distribution (Lauer et al. 1992a). This feature has also been reported in M32 (Lauer et al. 1992b) and NGC 7457 (Lauer et al. 1991).

Our *HST* observations of NGC 1316 and NGC 3998 give us a way to probe these questions. We also observed a "control sample" of radio-quiet ellipticals. These results will be reported in a separate paper.

The paper is organized as follows: we first describe the observations (§ 2); we then describe our data analysis and report the results (§ 3); we discuss the implications of these results in § 4; and we summarize the paper in § 5.

2. OBSERVATIONS

NGC 1316 and NGC 3998 were observed with the FOC in high-resolution mode (f/96; 1 pixel = 0".022) through several filters (neutral density wide-band filters were also used). The log of the observations including the filters used with their effective λ and bandpass, and exposure times are given in Table 1. The conversion factors between counts in a given filter and flux densities are given in Table 2. For a description of the characteristics of the FOC and the filters used, see the FOC handbook (Paresce 1992). These observations results in 512 × 512 pixel (11" × 11") fields including the central regions of these galaxies with good signal-to-noise ratio data for the two exposures of NGC 1316 and the F480LP exposure of NGC 3998. However, a bright nuclear point source in NGC 3998 caused the central pixels to be overexposed in the F342W and in the UV F175W exposures. Count rates of 2.0 and 2.5 counts s^{-1}, respectively, were detected in the central pixels of these exposures, implying that these pixels are "noticeably nonlinear" with some of the surrounding pixels becoming nonlinear as well (Greenfield et al. 1992).

3. DATA ANALYSIS

3.1. *Images*

The images used for our analysis were photometrically and geometrically corrected by the standard pipeline processing (Paresce 1992). Further analysis of these calibrated images was done using the STSDAS and XRAY packages of IRAF. The NGC 1316 images are shown in Figures 1*a* and *b* (Plate 1). The F480LP image shows an extended slightly asymmetric central region. The F175W image suggests the presence of pointlike nuclear emission. The three NGC 3998 images look similar, with a circularly symmetric extended surface brightness, and a central point-like source. We show the F480LP image in Figure 1*c*. To obtain a better visual representation of the data, these images were deconvolved using the Lucy-Richardson technique and point spread functions (PSF) from the *HST* library (see Appendix A for details). The deconvolved images are shown in Figures 1*d* and 1*e* for NGC 1316 and in Figure 1*f* for NGC 3998. Contour plots of the deconvolved data smoothed with the PSF are shown in Figures 2*a*, 2*b*, and 2*c*. Contour plots of the deconvolved data smoothed with a 2 pixel Gaussian are shown in Figures 2*d*, 2*e*, and 2*f*. These contour plots confirm the visual impression given by the

TABLE 2

CONVERSION FACTORS

Filter	PHOTFLAM[a]
F480LP	9.842×10^{-17}
F342W	6.769×10^{-18}
F175W	4.651×10^{-17}

[a] PHOTFLAM is the flux density (ergs cm^{-2} s^{-1} $Å^{-1}$) that produces a count rate of 1 per second with the *HST* observing mode. Multiply an observed count rate by PHOTFLAM to get the mean broad-band flux density of the target in the passband with which the target was observed. To find *HST* magnitude use: mag = $-2.5 \times \log(F) - 21.1$.

1994ApJ...434...67F

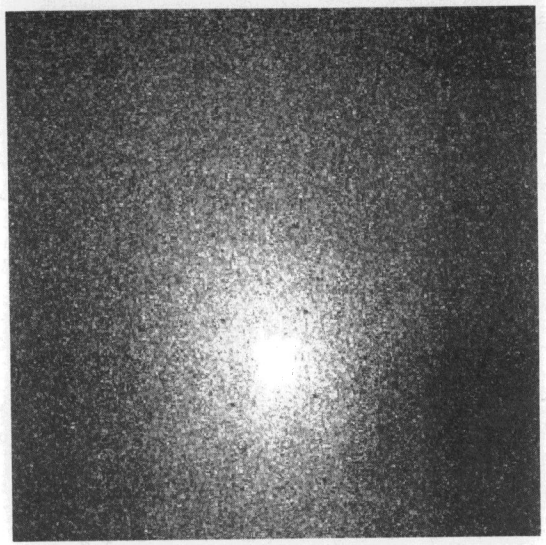

FIG. 1*a*

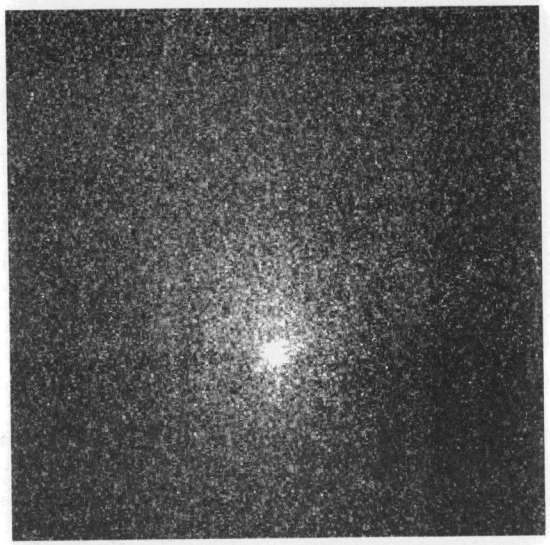

FIG. 1*b*

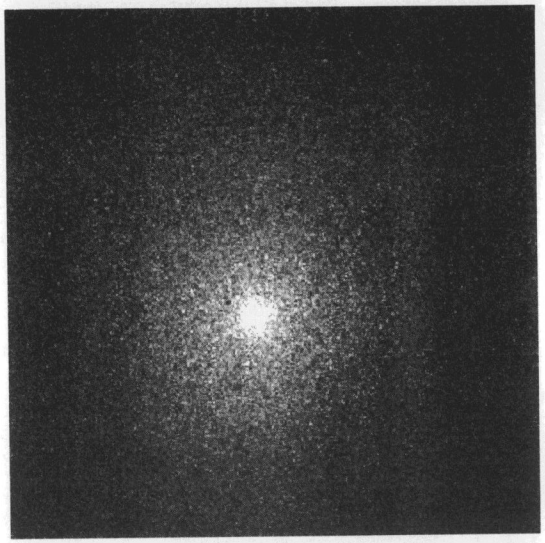

FIG. 1*c*

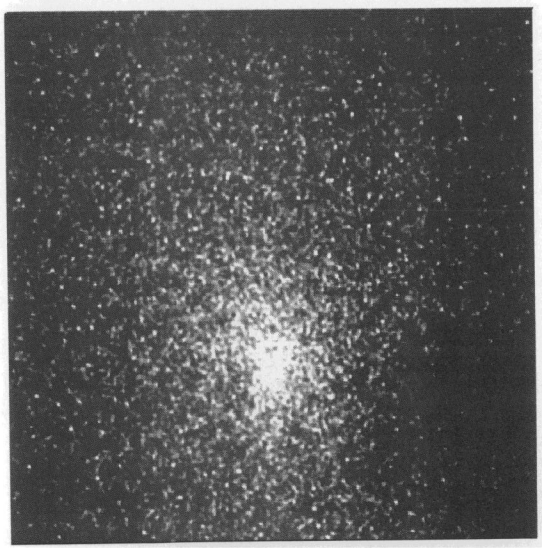

FIG. 1*d*

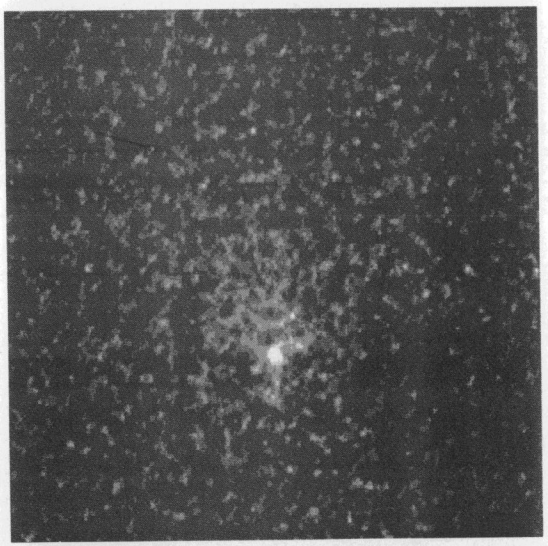

FIG. 1*e*

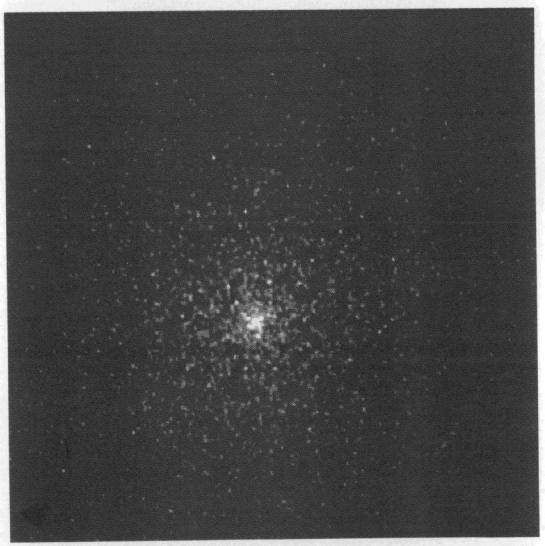

FIG. 1*f*

FIG. 1.—Galaxy images before and after deconvolution. The intensities are on a logarithmic scale. (*a*) NGC 1316 F480LP raw, (*b*) NGC 1316 F175W raw, (*c*) NGC 3998 F480LP raw, (*d*) NGC 1316 F480LP deconvolved, (*e*) NGC 1316 F175W deconvolved, and (*f*) NGC 3998 F480LP deconvolved.

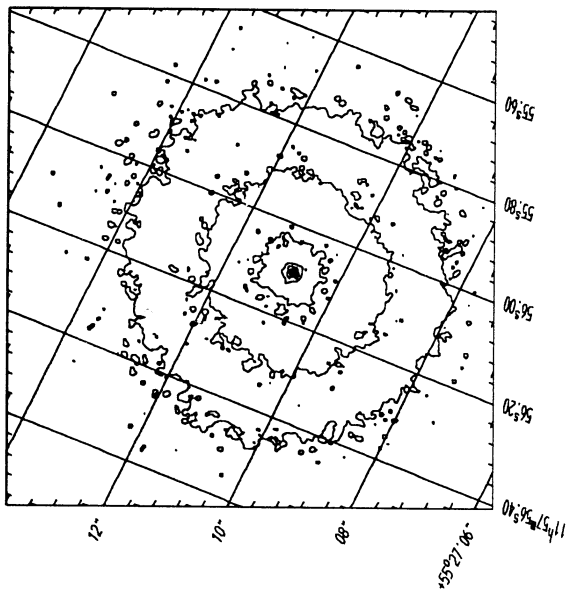

FIG. 2c

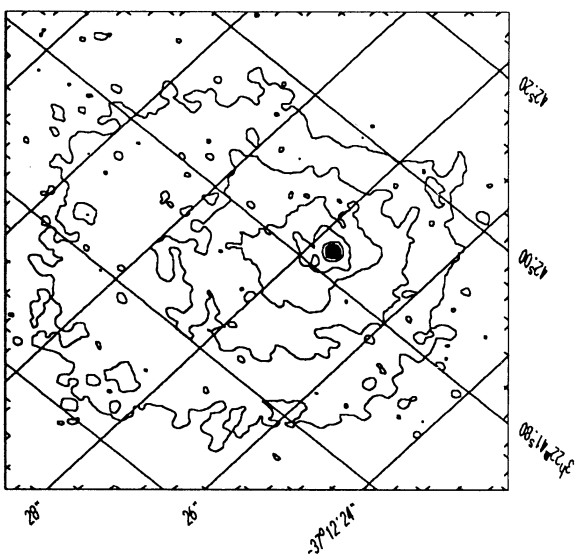

FIG. 2b

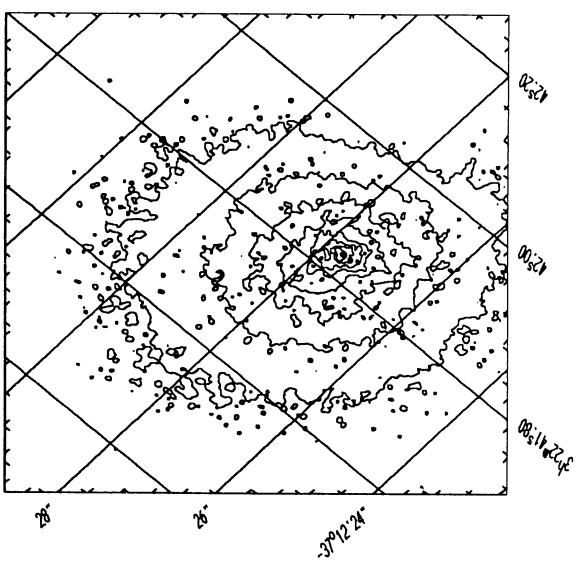

FIG. 2a

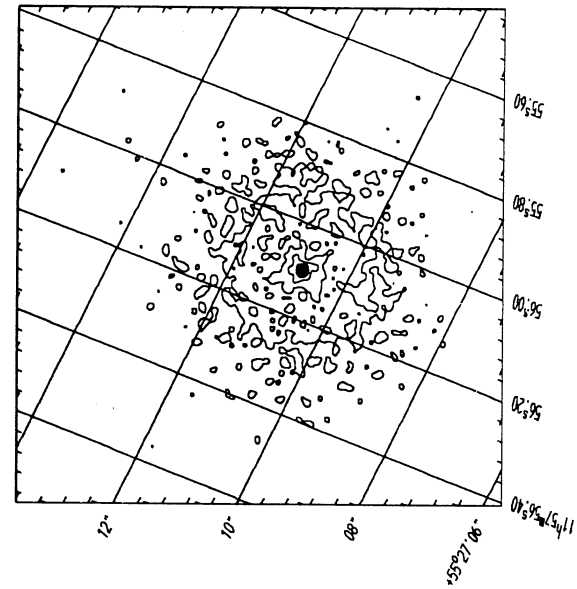

FIG. 2f

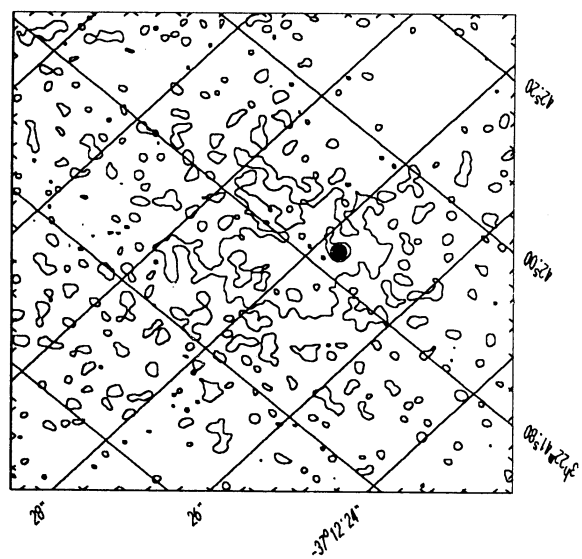

FIG. 2e

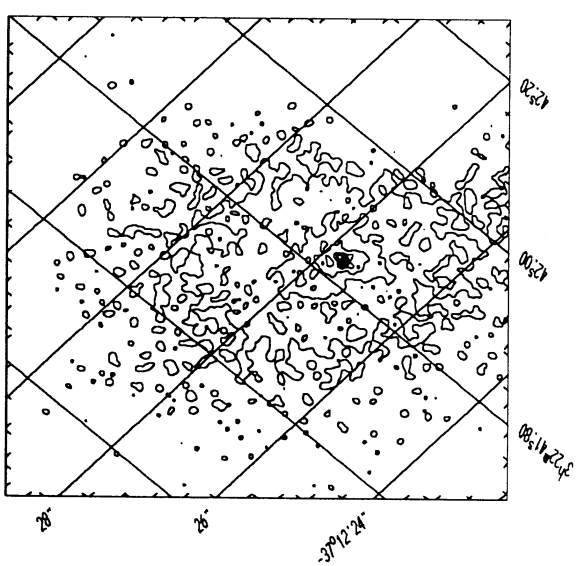

FIG. 2d

FIG. 2.—Contour plots of deconvolved images smoothed with the appropriate PSF: (*a*) NGC 1316 F480LP, (*b*) NGC 1316 F175W, and (*c*) NGC 3998 F480LP; (*d*), (*e*), and (*f*): same as above but smoothed with a 2 pixel Gaussian.

TABLE 3

POSITIONS OF EMISSION CENTROIDS AND CENTERS OF "TRIMMED" IMAGES

OBJECT	FILTER	CENTER OF EMISSION		CENTER OF 384 × 384 REGIONS	
		R.A.	Decl.	R.A.	Decl.
NGC 1316	F480LP	$03^h22^m41^s.84$	$-37°12'27''.73$	$03^h22^m41^s.76$	$-37°12'28''.80$
	F175W	03 22 41.84	−37 12 27.75	03 22 41.77	−37 12 28.66
NGC 3998	F480LP	11 57 56.09	+55 27 10.90	11 57 56.10	+55 27 11.69
	F342W	11 57 56.08	+55 27 10.83	11 57 56.10	+55 27 11.69
	F175W	11 57 56.09	+55 27 10.92	11 57 56.08	+55 27 11.77

NOTE.—All R.A. and decl. measurements are J2000.

unprocessed data and show clearly the presence of unresolved sources at the peak of more extended surface brightness distributions.

3.2. *Surface Brightness Profiles*

We used both calibrated images and deconvolved images to derive surface brightness profiles. We chose to use the calibrated images for further quantitative analysis, to avoid uncertainties that may be introduced by the deconvolution, which we cannot quantify. However, we often used the radial profiles obtained from the deconvolved images as a first guess for subsequent analysis.

We produced surface brightness radial profiles centered on the brightest pixel in the image, which coincided with the centroid of the emission as shown by the contour plots (see Table 3). We excluded pixels associated with the reseau marks. We followed two methods to generate these profiles:

1. We used the profile generating software in the IRAF XRAY package to find the number of counts in each of a series of concentric annuli placed at the center of emission, and dividing them by the appropriate area. The profiles are shown in Figure 3, with magnitudes calculated using the conversion factors in Table 2. The errors in the plots take into account only the counting statistics (the FOC is a photon counting instrument).

2. We used the STSDAS isophote package to fit elliptical isophotes to the images and derive surface brightness profiles. In this software the errors are not the Poisson errors ($N^{1/2}$), but are the RMS of the pixel-to-pixel variations. The result is that these errors tend to be larger, especially in the outer low surface brightness areas, where, however, there is still a large number of detected photons and therefore a large signal-to-noise ratio (in the counting statistics sense).

For NGC 3998 we found that the isophotes were nearly circular, with an average ellipticity of around 0.1 for all three filters. This low ellipticity can also be deduced from the contour plots of this galaxy (Fig. 2). In addition, we generated radial profiles in six image slices separated by 30°. The profiles are very similar, implying a high degree of axial symmetry. We thus used circular regions for our radial profiles of NGC 3998 in the remainder of the analysis. NGC 1316 presents a more complex situation. The brightness distribution is not symmetric, as can be seen by comparing radial profiles taken along two perpendicular axes (Fig. 4*a*). The structure of the galaxy is so irregular that neither circular nor elliptical isophotes fit the image well. However, the elliptical approximation and the cir-

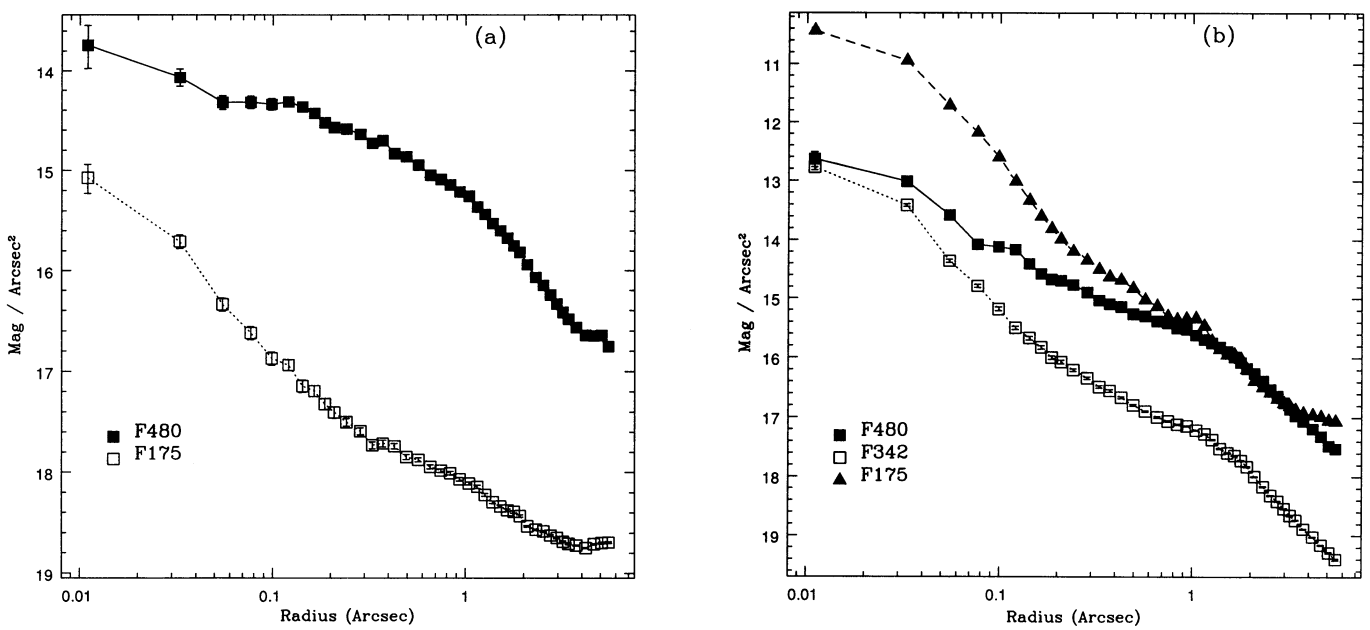

FIG. 3.—Surface brightness radial profiles for (*a*) NGC 1316 and (*b*) NGC 3998. The annuli used to produce the profiles had outer radii of 1, 2, 3, 4, 5, 6, 7, 8, 9, 10, 12, 14, 16, 18, 21, 24, 28, 32, 36, 40, 45, 55, 60, 66, 72, 78, 84, 90, 100, 110, 120, 130, 140, 150, 160, 180, 200, 220, 240, and 260 pixels.

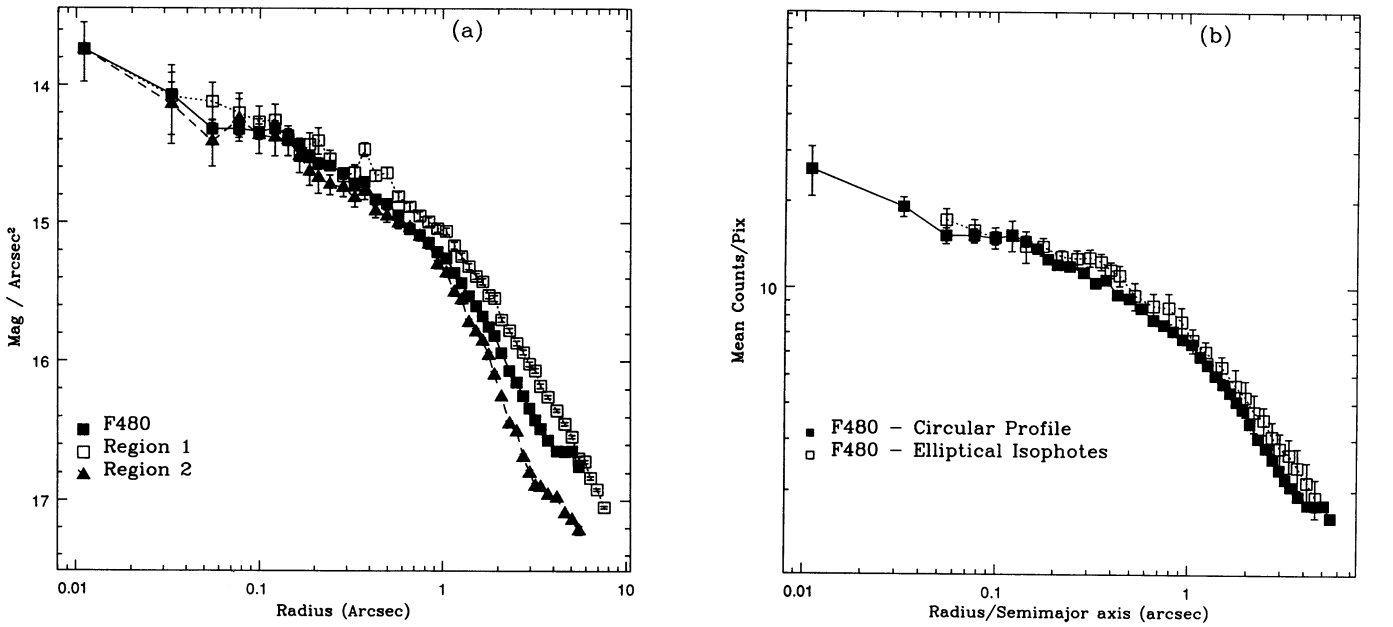

FIG. 4.—(*a*) Comparison of circularly averaged profile of NGC 1316 with two profiles taken at different azimuthal angles. Region 1 is along the apparent major axis of the emission, and Region 2 is perpendicular to it. (*b*) Comparison of radial profiles obtained by using circular annuli and elliptical isophotes. The errors on the isophotal profile are the rms errors in the surface brightness of the fit.

cular approximation give similar surface brightness profiles (Fig. 4*b*). We used the circular approximation for our model-fitting analysis (see § 3.3), and then checked the best-fit model against the elliptical isophotes. We also did a separate fit of the higher surface brightness "region 1" slice of Figure 4*a*; if the asymmetry is due to extinction, this may give a closer approximation to the "unabsorbed" distribution.

3.3. *Model Fitting*

To derive the surface brightness parameters, we fitted the surface brightness profiles to various combinations of a modified Hubble law or approximated King profile ("King": $\Sigma_K/[1 + (r/r_c)^2]$), a centrally flattened power law ($\Sigma_{pow}/[1 + (r/r_{pow})]^{\alpha}$), and a central point source, convolved with the appropriate *HST* PSF (see Appendix A). The following parameters were varied: "King" core radius (r_c), "King" normalization (Σ_K), point source normalization (Σ_{pt}), power-law index (α), power-law normalization (Σ_{pow}), and power-law core radius (r_{pow}). Since our profiles are from the innermost regions of the observed galaxies, where we observe an overall range of surface brightness of slightly above 1 dex (if we exclude central unresolved spikes), our "King" profile is a reasonable approximation of a whole family of King models (see Figs. 4–9 of Binney & Tremaine 1987). Our choice of models gives us a way to parameterize deviations from flat core surface brightness distributions that may suggest the presence of a central massive object (e.g., Lauer et al. 1992a).

The typical background rate for the f/96 configuration of the FOC is 6×10^{-4} counts pixel^{-1} s^{-1}, although values of up to 5 times this number are seen through the *HST* orbit (Greenfield et al. 1991). Because the field of view of the FOC is so small relative to the area covered by the galaxies, it is difficult to determine the true background level. The UV exposures are clearly background dominated at the outer radii because the surface brightness profile is flat (see Fig. 3). We approximated the field background in the F480LP exposures by adding a flat term to our model fitting.

We fitted the F480LP images using the following procedure. We first used surface brightness profiles derived from the deconvolved images (§ 3.1) to determine the initial guesses for the model parameters. We then followed an iterative procedure in which (1) we created a parameter space for a certain range of the varied parameters; (2) we used a χ^2 goodness of fit test to compare the radial profiles of the image and the convolved model; (3) we found the best fit in the parameter space and then used 2 σ confidence contours (Avni 1976; Press et al. 1988) to determine the range for the next iteration. Once a minimum was found for a given model, we added to the model a flat background term and repeated the search. Details on the fitting procedure and on the results are given in Appendix B. This procedure is quite time consuming but has the advantage of giving fairly unbiased results, compared with other approaches requiring unavoidably subjective data manipulation, as, for example, removing the central unresolved point source "by hand."

A simplified procedure was followed for the F175W image of NGC 1316 because of large uncertainties in the evaluation of the stellar surface brightness distribution at larger radii (see Appendix B). We did not fit models to the F342W and F175W images of NGC 3998 because the high count rate of the central point source causes the central pixels to be saturated.

The best-fit models are summarized in Table 4 for the F480LP and F175W images of NGC 1316, and for the F480LP image of NGC 3998. The results are discussed in detail in Appendix B. The errors on the parameter values are the maximum 2 σ errors found in the parameter space (Avni 1976; Press et al. 1988). However (see Appendix B), these uncertainties are likely to be underestimated, and may correspond to the 68% confidence level.

TABLE 4

RESULTS OF MODELLING[a]

Galaxy	Filter	Model	χ^2_ν	ν	Normalization (counts)	r_c (arcsec)	r_c (pc)[b]	α	Background (counts pixel^{-1})
NGC 1316	F480LP	1. King	1.96	31	4.6 ± 0.3	0.79 ± 0.088	104 ± 11.5	...	0.07 ± 0.01
		+ Power			113 ± 4	0.020 ± 0.0011	2.6 ± 0.14	0.805 ± 0.01	
		2. Power	1.95	33	48.5 ± 1	0.17 ± 0.0044	22 ± 0.58	1.055 ± 0.01	0.15 ± 0.0125
		3. Power	1.89	33	48.5 ± 1	0.17 ± 0.0044	22 ± 0.58	1.055 ± 0.01	0.15[c]
		+ Point			300 ± 300	...	...	...	
		4. Power[d]	1.43	36	40 ± 4	0.21 ± 0.022	27 ± 2.8	0.935 ± 0.01	$0.03^{+0.09}_{-0.03}$
	F175W	1. Power	...	...	15	0.20[c]	26[c]	1.07[c]	
		+ Point			5500	...	...	...	
NGC 3998	F480LP	1. King	1.79	32	4 ± 0.1	1.7 ± 0.044	280 ± 7.5	...	0.3 ± 0.025
		+ Power			230 ± 20	0.022 ± 0.0011	3.7 ± 0.19	1.31 ± 0.02	
		+ Point			3700 ± 600	...	...	...	
		2. Power	18.8	35	121	0.039	6.5	0.995	
		+ Point			2200	...	...	...	

[a] Errors are "formal" 2 σ errors (see § 3.3). Given the results of our fits (see § 3.3.3) they are approximately equivalent to 1 σ errors.
[b] Assumed distances are 27 Mpc for NGC 1316 and 35 Mpc for NGC 3998.
[c] Fixed.
[d] Fit to high-flux azimuthal area ("Region 1" in Fig. 4*a*).

4. RESULTS

4.1. *Extended Surface Brightness Parameters*

4.1.1. *NGC 1316*

The best-fit models 1. and 2. of Table 4 for NGC 1316 F480LP are shown in Fig. 5. The average surface brightness distribution can be entirely explained with a centrally truncated power law distribution (model 2.), with no need for an underlying flatter core "King" component. However, models 1. and 2. predict substantially different "intrinsic" central surface brightness profiles at the inner radii (Fig. 6).

The uncertainty on the behavior of the central surface brightness is increased by the likely presence of extinction, suggested by ground-based surface photometry (Schweizer 1981). A comparison of the *HST* FOC and ground-based surface brightness profiles of NGC 1316 (Schweizer 1981) is shown in Fig. 7. The $\lambda_{\rm eff}$ of the F480LP filter is intermediate between those of the filters used by Schweizer, although closer to that of the B_2 filter. The two Schweizer profiles have been renormalized to make them match the FOC data at large radii. As can be seen from the figure, the data and our best-fit prediction agree well with the Schweizer profiles outside 2″. In the inner regions, our F480LP profile is reasonably close to the B_2 profile (in fact, in Fig. 7 the points in the F480LP profile hide those in the B_2 profile between 0.″6 and 5″), in agreement with what could be expected from the different filter bandpasses. Schweizer (1981) ascribed the difference between the two profiles to extinction in the central regions of NGC 1316.

Extinction, however, must be patchy. In particular, the presence of an UV-bright unresolved nuclear source (§ 4.2) suggests a fairly extinction-free line of sight to the nucleus. If significant extinction is present in the center of NGC 1316, it could be responsible for the irregularities in the central pixels of the inner surface brightness distribution (see Fig. 2). Extinction could also result in a flattening of the profile in the center, if it becomes relatively more severe at smaller radii, as suggested by Figure 7. For these reasons, our results on slope and core radius of the central surface brightness should probably be regarded respectively as lower and upper limits on the intrinsic values.

4.1.2. *NGC 3998*

In NGC 3998, a "King" component and a central power law are both required to fit the F480LP profile, in addition to an unresolved central source (Fig. 8; see Appendix B); a power-law–only model for the extended surface brightness distribution cannot fit the data (see Table 4). Figure 9 shows a comparison of the observed surface brightness profile (in the F480LP filter) of NGC 3998, with the best-fit extended components ("King" + power-law), before and after convolution with PSF. This multicomponent morphology is reminiscent of that of M87 (Young et al. 1978; Lauer et al. 1992a). However, the power-law component is much steeper than that present in M87 (the M87 $\alpha = 0.26$; Lauer et al. 1992a) and may be truncated at the small radii (~ 3 pc; see Table 4), while in M87 no central flattening has been reported.

Figure 10 shows a comparison between the observed surface brightness profile, from which the best-fit point-source and "King" components have been subtracted, and a set of power laws with $r_{\rm pow}$ ranging from 0.″0055 to 0.″039 (note that the two innermost points are far below the best-fit power law; these points were partially saturated—see § 2—so they fall below the PSF prediction). Figure 10 shows that the distribution of points inwards of 0.″2 excludes $r_{\rm pow} \leq 0.''011$ (1.8 pc for $D = 35$ Mpc). However, this is the region where a proper estimate of the central PSF is essential (see also Crane et al. 1993). We believe that our procedure is the best approach one can follow with these data. However, we urge reobserving this galaxy after the *HST* optics are corrected to confirm this point. Also, with the present data, we cannot comment on the possible presence of extinction in the central regions of NGC 3998.

4.2. *Point Source Fluxes and Luminosities*

As discussed above, we detect unresolved central sources in the UV F175W exposure of NGC 1316 and in all our exposures of NGC 3998. Table 5 lists count rates, fluxes, and luminosities of these pointlike sources. Details on the point source count extraction are given below. Count rates were obtained by dividing the source counts by the exposure times; and fluxes were then calculated by using the conversion factor in the image header, which takes into account the filter transmissions

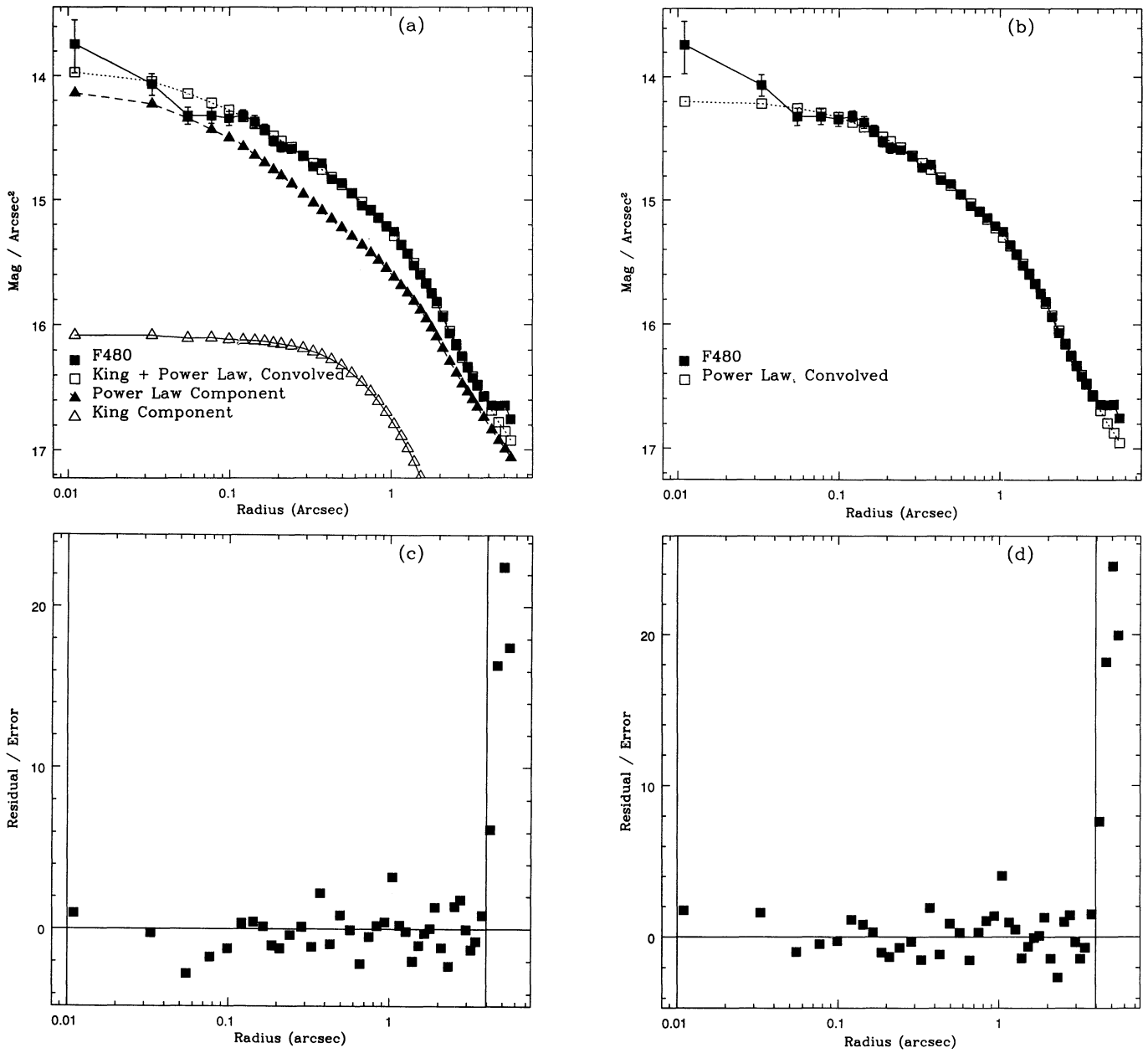

FIG. 5.—Final models obtained by fitting to the NGC 1316 F480LP image. (*a*) "King" + power law model showing the relative intensities of the two components. The background level is 20.1 mag arcsec^{-2}. (*b*) Power-law model. The background level is 19.3 mag arcsec^{-2}. (*c*) and (*d*) The residuals from fitting the "King" + power-law model and power-law–only model. The vertical lines delineate the range used in the fitting.

TABLE 5

POINT SOURCE PARAMETERS

Image	Count Rate (counts s^{-1})	Flux (ergs cm^{-2} s^{-1} Å^{-1})	Flux in Band (ergs cm^{-2} s^{-1})	Luminosity in Band (ergs s^{-1})
NGC 1316 F480LP	<0.7	$<6.5 \times 10^{-17}$	$<4.7 \times 10^{-14}$	$<4.1 \times 10^{39}$
NGC 1316 F175W	3.3	1.6×10^{-16}	1.1×10^{-13}	9.2×10^{39}
NGC 3998 F480LP[a]	6.8	6.7×10^{-16}	4.8×10^{-13}	5.2×10^{40}
NGC 3998 F480LP[b]	7.7	7.5×10^{-16}	5.4×10^{-13}	5.8×10^{40}
NGC 3998 F480LP[c]	12.9	1.3×10^{-15}	9.3×10^{-13}	1.0×10^{41}
NGC 3998 F342W[b]	>61.5	$>4.2 \times 10^{-16}$	$>2.9 \times 10^{-13}$	$>3.1 \times 10^{40}$
NGC 3998 F342W[c]	>99.5	$>6.7 \times 10^{-16}$	$>4.7 \times 10^{-13}$	$>5.1 \times 10^{40}$
NGC 3998 F175W[b]	>217.0	$>1.0 \times 10^{-14}$	$>6.8 \times 10^{-12}$	$>7.3 \times 10^{41}$
NGC 3998 F175W[c]	>209.5	$>9.8 \times 10^{-15}$	$>6.6 \times 10^{-12}$	$>7.1 \times 10^{41}$

[a] From model fit.
[b] Subtracting from data best-fit extended component.
[c] Extracting counts from circle and using adjacent annulus for evaluating the background (see text).

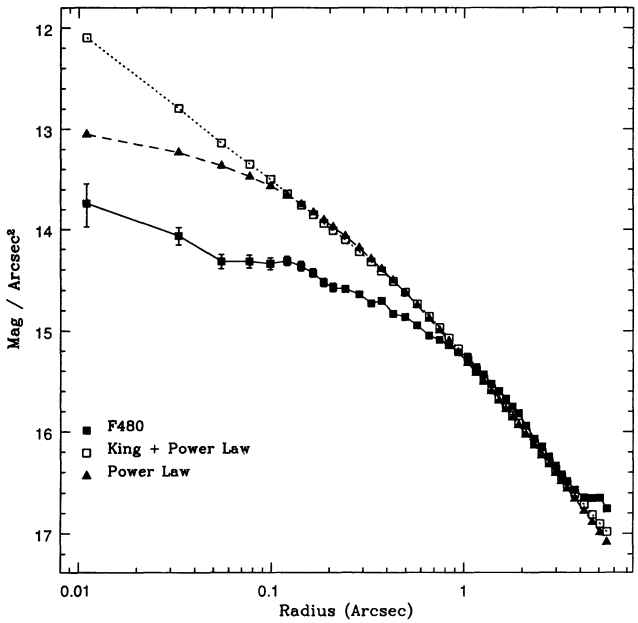

FIG. 6.—Comparison of NGC 1316 F480LP observed profile with unconvolved best-fit "King" + power-law and power-law model profiles.

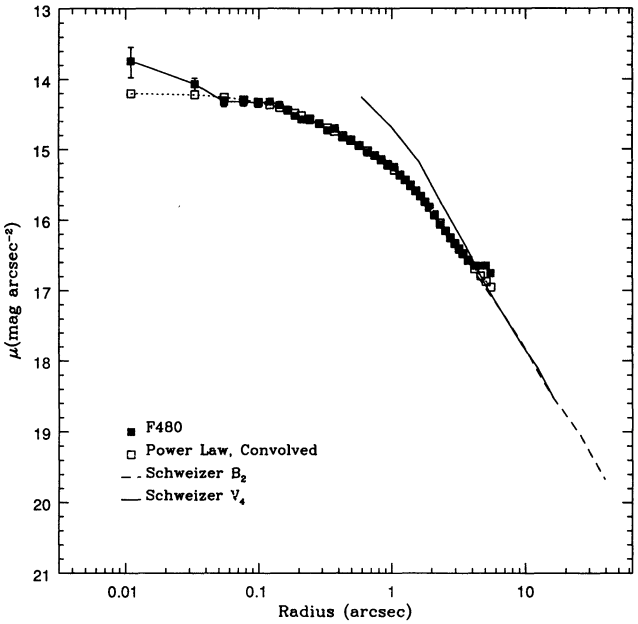

FIG. 7.—Comparison of NGC 1316 F480LP observed profile and best-fit power-law model with ground-based observations from Schweizer (1981). The Schweizer profiles have been renormalized to match the FOC profiles at large radii.

(Table 2; see Paresce 1992). Luminosities were calculated using the distances given in Table 4.

For NGC 1316 we estimated the point source counts from the best-fit models of Table 4. The F480LP point-source values are given as upper limits in Table 5 from the power-law + point source fit, because a central point source is statistically marginal in this model, and is certainly not required in the case of a "King" + power-law model. Our fit to the F175W NGC 1316 profile is shown in Figure 11; the surface brightness is almost entirely dominated by a central unresolved source.

For NGC 3998 we also used the results of Table 4 to estimate the point source counts in the F480LP exposure. For the F342W and F175W images (which are overexposed; see § 2), we estimated lower limits to the point source fluxes by two different methods:

1. Taking the power law and "King" components obtained by fitting the F480LP exposure and adjusting the component normalizations so that the model profile matched the observed profile at large radii. For the F175W exposure, we added a

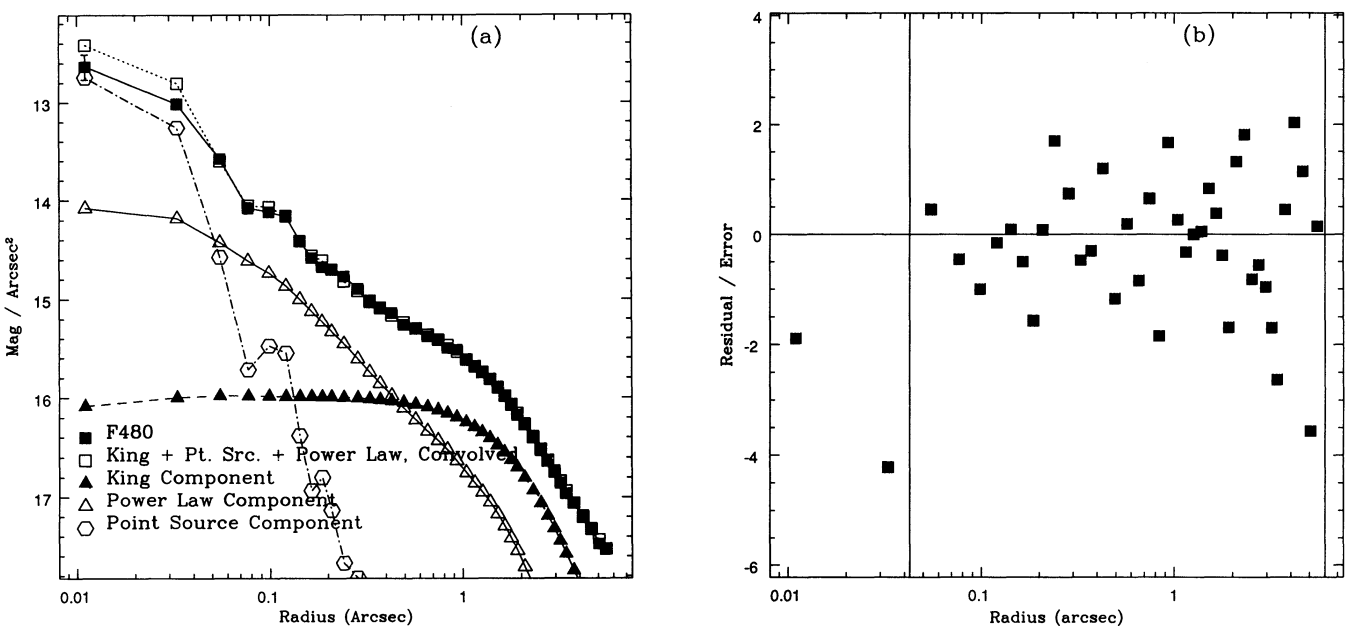

FIG. 8.—(*a*) "King" + power-law + point source model fit to the NGC 3998 F480LP image showing the relative intensities of the three components. The background level is 18.5 mag arcsec^{-2}. (*b*) Fit residuals. The vertical lines delineate the range used in the fitting.

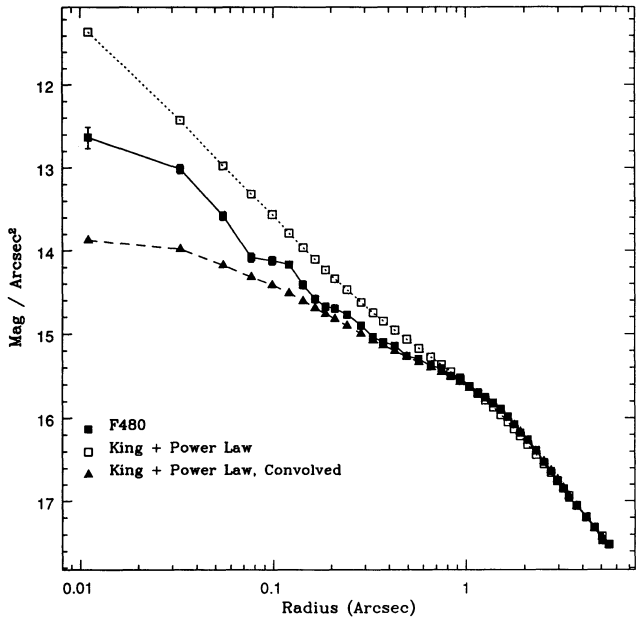

FIG. 9.—NGC 3998 F480LP observed profile with best-fit "King" + power-law component.

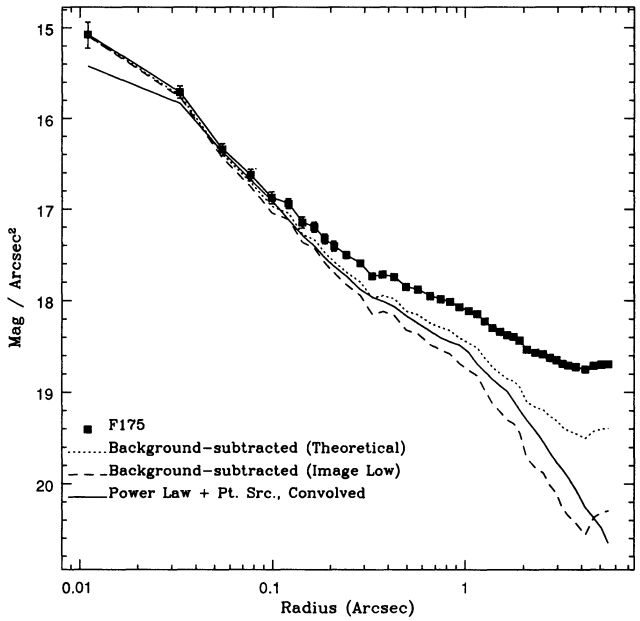

FIG. 11.—The power-law + point source model obtained by fitting to the NGC 1316 F175W image. The component normalizations have been adjusted to make the model profile consistent with the background-subtracted profiles.

constant background of 1 count pixel^{-1} to account for the high field background in the observed image. We assumed that any excess emission at small radii was contributed by the central point source, and we corrected for the estimated PSF scatter outside our "source" radius.

2. Summing the excess counts inside radii of 0".2 (F342W) and 0".4 (F175W) and then correcting for the fraction of counts scattered outside these radii by the PSF.

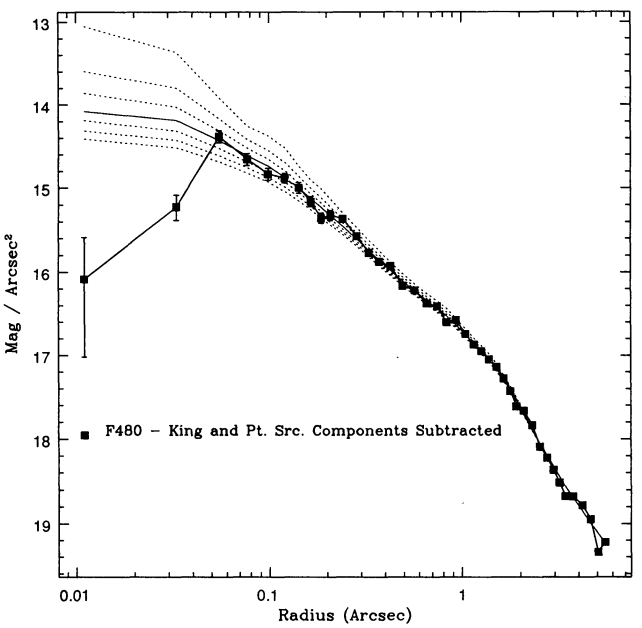

FIG. 10.—NGC 3998 F480LP observed profile with best-fit "King" and point source components subtracted. The solid line represents the best-fit power-law component, with a core radius of 0".022. The dashed lines are the power-law component with core radii ranging from 0".0055 (*top line*) to 0".039 (*bottom line*) in steps of 0".0055.

We list both values in Table 5; for completeness we give also the F480LP count rates obtained with these two methods. Typically the second approach gives the higher possible estimate of the central point source counts whenever an extended surface brightness component is important, because it assumes a flat stellar surface brightness distribution at small radii.

Fluxes and luminosities in Table 5 are not corrected for absorption, because we have no way of estimating the intrinsic nuclear extinction. Both galaxies are relatively unaffected by galactic extinction. Table 5 shows clearly that the unresolved sources in the two nuclei are both UV-bright. We believe that this conclusion is not affected significantly by red-leaks in the F175W filter because the point source is not detected in the F480LP image in the case of NGC 1316 and has a significantly lower count rate in this filter in the case of NGC 3998. The opposite is true in the case of the extended galaxy emission (see Table 4). Given the uncertainties in the fits due to the subtraction of an extended galaxy component and saturation of the peak emission in some cases (see § 3.2), it is not meaningful to establish an upper limit on the extent of the unresolved central emitting region using χ^2 fitting techniques. However, it is clear from visual inspection of the surface brightness profiles that we can exclude uniform emitting regions of 0".2–0".3 radius. This corresponds to a fairly conservative radius of $\sim$3 pc for the central emitting regions.

5. DISCUSSION

5.1. *The Central Sources*

Our observations have established the presence of UV-bright unresolved sources ($r < 3$ pc) at the nuclei of NGC 1316 and NGC 3998. Here we compare our results with those of previous observations and we discuss their implications for the nature of these galaxy nuclei.

In both galaxies there have been previous reports of the presence or possibility of unresolved nuclear emission. In NGC 1316, the possibility of a highly reddened central point source

had been raised by Schweizer (1981) to explain an excess seen in the inner part of the redder of his two images of this galaxy. As discussed above, our "redder" image is in a wavelength range close to that of Schweizer's blue filter, and we do not have convincing evidence of a point source in this image. The point source is instead prominent in the UV exposure. The presence of this UV emission suggests that the source we detect may not be associated with the excess red emission found by Schweizer, unless its emission spectrum is either extremely UV bright (in the presence of extinction), or has intrinsic peaks in both red and UV bands. It is clear that high-resolution imaging of this nuclear region in a redder band is needed to explore further this question. Nuclear UV line emission in NGC 3998 has been reported by Reichert et al. (1992), but this nucleus had not been previously imaged. *HST* resolution was needed to detect the nuclear source above the bright stellar field. We see this source in all three filters used to observe this galaxy but unfortunately our F342W and F175W images are overexposed at the nucleus. So, we can only establish lower limits to the flux of the point source in these two bands. A comparison of our fluxes with those of Reichert et al. suggests that the nuclear source is more UV-bright that previously reported. However, the large aperture of *IUE* would make the stellar field subtraction of Reichert et al. rather uncertain.

With our data (Table 5) we can set lower limits of $\geq 10^{40}$ ergs s^{-1} and $>7 \times 10^{42}$ ergs s^{-1} to the UV/bolometric luminosities of the NGC 1316 and NGC 3998 nuclei, respectively. This emission could be explained with a cluster of O stars (a few in NGC 1316; a few hundred in NGC 3998). However, it is also possible that the nuclear sources are the optical/UV counterparts of the radio-emitting active nuclei. In the case of NGC 3998 this hypothesis is supported by the emission-line optical-UV LINER spectrum. The bolometric luminosity of the NGC 1316 nucleus is comparable with that of the nucleus of NGC 4395, the lowest luminosity Seyfert nucleus yet discovered (Filippenko & Sargent 1989), while the NGC 3998 nucleus is about 10 times more luminous than the nucleus of M81 (see Fabbiano 1988 and references therein).

In both galaxies there is evidence of emission line circumnuclear disks (Ford et al. 1986; M. Franx 1993, private communication), which might be effective in channeling gas toward the nuclei. If we assume that the nuclear emission is due to a single object, we can derive firm lower limits on the mass of this object, using the Eddington limit. These limits are of $>75\ M_\odot$ for NGC 1316 and $>10^4\ M_\odot$ for NGC 3998, suggesting the presence of massive black holes. We point out that, within our model assumption, these limits are conservative because our data are not corrected for nuclear extinction.

To obtain further clues on the nature of these nuclear sources, we compare their flux distributions with those of M81 and two representative bright AGNs: the radio-loud 3C 273, and the radio-quiet Mkn 205 (Fig. 12, adapted from Fabbiano 1988). Note that the fluxes plotted for the nuclei of NGC 1316 and NGC 3998 are not corrected for extinction. The IR points of NGC 3998 are from Knapp, Gunn, & Wynn-Williams (1992), and the radio points for both NGC 1316 and NGC 3998 (nuclei) are from Fabbiano et al. (1989). The V point of M81 is from the measurement of the nuclear source with the *HST* FOC of Crane et al. (1993). Figure 12 suggests that there may be an overall resemblance between the spectral distributions of the nucleus of M81 and high-luminosity AGNs, while the nuclear source in NGC 3998 has a significantly different steep optical-UV spectral distribution. From Table 5, we can derive

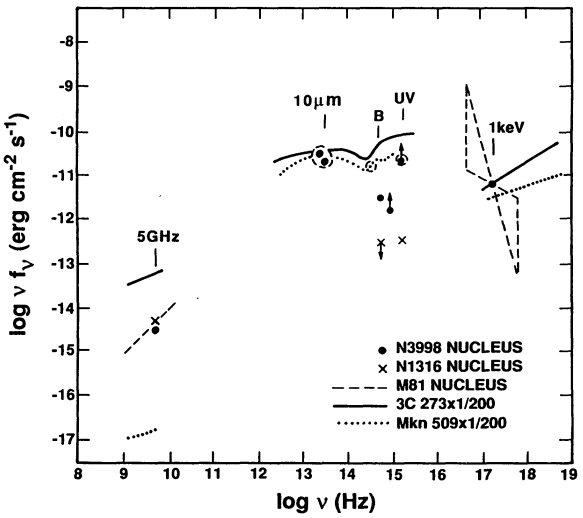

FIG. 12.—Energy distribution of the nuclear sources of NGC 3998 and NGC 1316, compared with those of M81 and of two bright AGNs (see text).

the *B–UV* slope of the nucleus of NGC 3998 and find $\alpha \geq 1.8$. This is much steeper than the accretion disk distribution used to model the emission of AGNs ($f_\nu \sim \nu^{1/3}$; e.g., Czerny & Elvis 1987), and could be consistent with the spectral shape of the low-frequency side of a blackbody. The *B–UV* slope of the NGC 1316 nucleus is less steep, but there is likely to be significant extinction in this source (Schweizer 1981), resulting in an intrinsically steeper spectrum. It is also possible that emission lines could affect these fluxes. It is clear that spectrophotometry of these nuclei is needed, before we can make definite conclusions on their nature.

5.2. *Are There Massive Black Holes in NGC 1316 and NGC 3998?*

The question that we sought to answer with these observations was are there massive black holes at the cores of elliptical galaxies with radio-emitting nuclei? Our observations are not enough in themselves to answer this question. The presence of unresolved nuclear emission may argue in a model-dependent way for black holes at the nuclei (e.g., Rees 1984), however, these sources are faint, and thus the black holes do not need to be extremely massive (see above).

As shown in §§ 3 and 4, the central surface brightness distributions of NGC 1316 and NGC 3998 do not follow a flat core "isothermal" profile. In both galaxies a centrally rising component of the surface brightness is needed to fit the data. The slope of this component is quite steep, with power-law indices ranging from 0.805 to 1.31. These slopes are steeper than those reported from *HST* observations of the massive black hole candidate M87 (0.26; Lauer et al. 1991a) and comparable to that of M32 (0.5 or 1.37; Lauer et al. 1992b), which could also host a massive black hole. Taken at face value, the results of our fits suggest that these power laws flatten at small radii, contrary to the expectancy in the case of massive central black holes.

However, in both galaxies there is considerable uncertainty in the central surface brightness parameters. In NGC 1316, both previous observations (Schweizer 1981), and the irregularity of the central surface brightness suggest a significant amount of extinction in the center. In this case, the central flattening may be the result of our observing in a relatively blue

window. In NGC 3998, extinction may also play a role, although there is no obvious evidence for it. Using our results of § 4 and the expressions in Schweizer (1979), we can estimate the average core properties of NGC 3998. Assuming a core surface brightness of 11 mag, we obtain an average core volume luminosity $\langle \lambda_B \rangle_c = 6.9 \times 10^5 (r_c/2\ \mathrm{pc})^{-1}\ L_{B,\odot}\ \mathrm{pc}^{-3}$, an average core density $\langle \rho \rangle_c = 2.0 \times 10^6 (\sigma_v/300\ \mathrm{km\ s}^{-1})^2 (r_c/2\ \mathrm{pc})^{-2}\ M_\odot\ \mathrm{pc}^{-3}$, and core mass–to–light ratio $\langle M/L \rangle_c \sim 3 \times (\sigma_v/300\ \mathrm{km\ s}^{-1})^2 (r_c/2\ \mathrm{pc})^{-1}\ M_\odot/L_\odot$. Clearly these estimates do not require a massive black hole. However, as discussed in § 4, our estimate of r_c is rather uncertain, due to the presence of a—possibly saturated—central point source. In our fit we used a PSF from the *HST* library observed with the same setup as ours. However, we did not obtain independently a PSF near in time to our observations. Uncertainties on the PSF would certainly affect our results.

Moreover, and this holds also for NGC 1316, we do not have measurements of the stellar velocity dispersion σ_v at these small radii. A centrally increasing σ_v would indicate the presence of a central dark mass concentration.

6. SUMMARY AND CONCLUSIONS

Observations of the central regions of NGC 1316 and NGC 3998 with the *HST* FOC have led to the discovery of stellar light distributions steeply rising toward the center. The central surface brightness distribution of NGC 1316 appears patchy and not axially symmetric, while that of NGC 3998 is smooth and mostly circular. Nuclear point sources were also discovered. In NGC 1316 this point source is clearly there only in the 1720 Å UV, while in NGC 3998 the point source is visible at all the observed wavelengths, although it is more prominent in the UV. Although we cannot exclude that these UV-bright unresolved sources may be due to clusters of O stars, at least in NGC 3998 the presence of an emission line nucleus (Reichert et al. 1992) supports the notion that we have imaged a low-luminosity AGN.

The central point source of NGC 1316 has a UV luminosity of the order of 10^{40} ergs s^{-1} (uncorrected for extinction), comparable with that of the faintest known active nucleus (NGC 4395; Filippenko & Sargent 1989). The point source in NGC 3998 appears two orders of magnitude brighter in the UV. The optical–UV flux distributions of the NGC 3998 nuclear source differs from that of the low-luminosity AGN at the nucleus of M81, being very steep, and resembling that of blackbody emission.

Fits of surface brightness profiles with a set of models convolved with the appropriate PSF show clearly that a flat-core profile such as an approximated King or Hubble law ($\sim 1/[1 + (r/r_c)^2]$) is not a suitable approximation in the inner regions. In NGC 1316 the data can be fitted with either a single–power-law distribution with a best-fit slope of 1.055, which flattens inward of $r_{\mathrm{pow}} = 0\farcs17$, or with an approximated King + power-law model. In the latter case, the power law component has a flatter slope (0.805) and also flattens at the center, although at smaller radii ($r_{\mathrm{pow}} = 0\farcs02$). However, the King component is very small, even at larger radii ($r > 1''$). The extended component of the surface brightness distribution of NGC 3998 is best fitted with an approximated King + power-law model. In this model, the best-fit power-law slope is 1.31, steeper than in the case of NGC 1316, and it is truncated at $r_{\mathrm{pow}} = 0\farcs022$.

The question that we sought to answer with these observations was are there massive black holes at the cores of elliptical galaxies with radio-emitting nuclei? Our observations are not enough in themselves to answer this question. The presence of unresolved nuclear emission argues in a model-dependent way for black holes at the nuclei (e.g., Rees 1984); however, these sources are faint, and thus the black holes do not need to be very massive. In NGC 1316, the central flattening of the stellar spike, that is required by our model fitting, may argue against a central massive black hole (see Lauer et al. 1992a). However, both previous observations (Schweizer 1981) and the irregularity of the central surface brightness of this galaxy strongly suggest a significant amount of dust in the center. In this case, the central flattening may be the result of extinction in our blue observing window. In NGC 3998, extinction may also play a role, although there is no obvious evidence for it, and there is the added uncertainty due to the presence of a central point source. In our fit we used a PSF from the *HST* library observed with the same setup as ours. However, we did not obtain independently a PSF near in time to our observations. Uncertainties on the PSF would certainly affect our results.

Concluding, these observations have demonstrated the presence of centrally steep stellar distributions in NGC 1316 and NGC 3998 and have imaged two very faint unresolved nuclei. Further work with *HST* will be needed to follow up these observations and to answer the still outstanding questions of the presence or less of nuclear massive black holes. We need to observe in a redder band in order to establish the effect of extinction in the central regions. We also need to obtain measurements of the central stellar velocity dispersion, to establish if there is an inward increase, as expected in the case of a central massive black hole (e.g., Sargent et al. 1978). The corrected *HST* optics will be extremely helpful in these future projects, to reduce the uncertainties in the innermost regions, where "all the action is."

This work was supported by the *HST* grant GO-2295.01-87A, by NASA grant NAGW-2681 (LTSA), and by NASA ASC contract (NAS8-39073). We thank Bill Sparks for advice on the setup of the observations; David Baxter and Dan Golombek for advice on the reduction of the *HST* data; Jeffrey Orszak for useful comments on programming techniques; Paul Eskridge and Martin Elvis for discussions on the scientific interpretations of the data; and Jay Gallagher for comments on the manuscript.

This research has made use of the NASA/IPAC Extragalactic Database (NED) which is operated by the Jet Propulsion Laboratory, California Institute of Technology, under contract with the National Aeronautics and Space Administration.

APPENDIX A

IMAGE PREPARATION AND DECONVOLUTION

We analyzed the calibrated images using IRAF and the STSDAS and XRAY packages. The images were trimmed to eliminate edge effects caused by the geometric correction, which results in an artificial "brightening" at the outer pixels. To simplify the later processing, we made the images square, with dimensions 384 × 384 pixels. These smaller images were centered as close as possible to the center of emission while still excluding the edge effects. The locations are listed in Table 3.

We deconvolved each of the images using the Lucy-Richardson technique (Lucy 1974; Richardson 1972) as implemented in the STSDAS package. For the observations made with the F480LP and F342W filters, we used observed PSFs from the library maintained by STScI. Because there is no observed F175W PSF in the library, we created a synthetic one by combining the PSF of the F152M filter with that of the F170M filter, multiplying them by weighting factors of $\frac{2}{3}$ and $\frac{1}{3}$, respectively. We had to prepare the PSFs for use in the deconvolution because the PSF fields (256 × 256 pixels) are smaller than the FOC images and show edge effects (D. Baxter 1992, private communication). We found a "typical" background count level for each PSF by sampling areas as far from the source as possible and then created a 1024 × 1024 pixel image consisting of Poisson noise with a mean value equal to the background count level found above. We then trimmed the edge effects from the image of the observed PSF. In order to preserve as many of the PSF data as possible, we chose the largest region that included the source yet excluded the edge effects. This trimmed image, with a typical area that was 70%–75% of the area of the original image, was then centered on the image consisting of the Poisson noise. The trimmed PSF was not added to the Poisson noise image, but rather replaced part of it. Thus the background level was consistent across the new combined image. We next subtracted the mean background value from each pixel, cut the size of the image to 384 × 384 pixels, and divided by the total number of counts in the image. The resulting PSF, with zero-mean noise, was used in the deconvolution.

We found that the agreement between the observed data and a convolution of the deconvolved data with the appropriate PSF improved as the number of iterations was increased. We found reasonable agreement if we performed 80 Lucy iterations in the deconvolution of each image.

APPENDIX B

MODEL FITTING

B1. NGC 1316 F480LP

We first tried an approximated King model plus a central flattened power law. King models have been found to fit the data adequately at larger radii (Schweizer 1981). Each of the four parameters was allowed to assume five equally spaced values, with the central value being that of the initial guess for that parameter. This gave us 625 models for each iteration of the fitting.

The first 22 iterations were performed with the compressed images. The last 27 iterations were performed on the full-resolution image (384 × 384 pixels of 0.″022 each). A field background parameter was included in the last 16 iterations. The best-fit model (Fig. 5*a*) had a χ^2 of 60.7 for 31 degrees of freedom. The background for this model was 0.07 counts pixel^{-1}, lower than the 0.27 counts pixel^{-1} level predicted for this exposure. Forcing a larger background term would result in a steeper power-law index. The residuals of the fit are shown in Fig. 5*c* and do not present any obvious trend, except for a few points near the edge, which were not included in the fit.

Almost the entire contribution to the model flux comes from the power-law component (see Table 4 and Fig. 5*a*). We thus decided to fit a single-component model, consisting only of a power law, to the data. It took 29 iterations to arrive at the final power-law model, the first seven using the compressed image. We once again used a grid with five values per parameter, giving us 125 models per iteration. We included a background parameter for the last six iterations. The best-fit model (Fig. 5*b*) had $\alpha = 1.055$, a core radius of 0.″17 (7.7 pixels) and a background level of 0.15 counts pixel^{-1}, closer to the theoretical background level of 0.27 counts pixel^{-1}. Again, the residuals are evenly scattered (Fig. 5*d*). The χ^2 was 64.3 for 33 degrees of freedom.

The innermost two bins suggest the possibility of excess emission over the model. However, the statistics are poor. We tried adding a central point source to the power-law model. For the first four iterations, we varied only the power-law normalization and point source intensity and kept the power-law index and core radius fixed. This allowed us to quickly find a good estimate for the two normalizations. For the last four iterations we varied the three power-law parameters and the point source intensity. We also added a field background component, which we kept fixed at the best-fit value from the power-law fitting. The final model had a χ^2 of 62.4 for 33 degrees of freedom and therefore there is no significant improvement in χ^2 that requires the presence of a central point source.

To estimate the effect of the asymmetry in the surface brightness on the model parameters, we performed a fit to the power-law model of the higher surface brightness azimuthal region of NGC 1316 (see § 3.2 and Fig. 4a). The results are also given in Table 4 and do not differ appreciably from those of the circularly averaged surface brightness profile, except for a lower value of reduced χ^2.

B2. NGC 3998 F480LP

We first fitted the image with a "King" model plus a central point source. We fitted a "King" model to the profile at large radii, which took 15 iterations, the last 12 of which included a background parameter. We then added to the best-fit "King" model a point source that would fit the surface brightness profile in the innermost two bins. This fit was inadequate because it did not

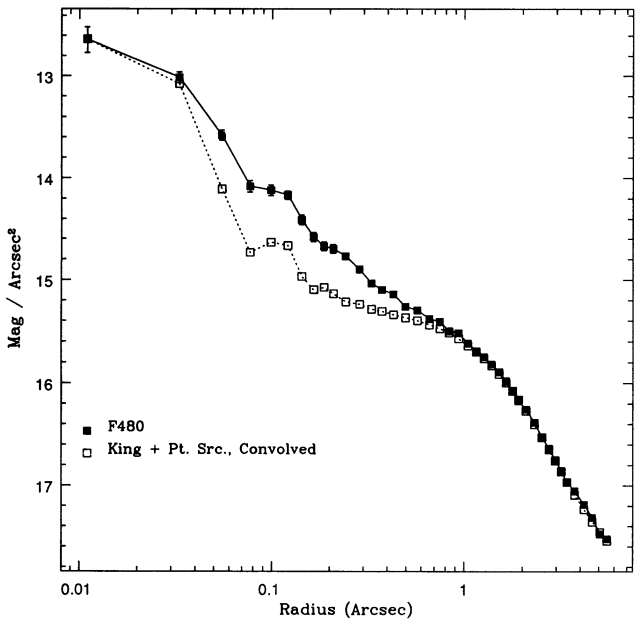

FIG. 13.—"King" + point source model fit to the NGC 3998 F480LP image. Note the inadequacy of the fit between 0".05 and 0".4.

properly account for the emission between approximately 0".05 and 0".4 (Fig. 13). The χ^2 was 1275 for 37 degrees of freedom. Even allowing the point-source component to be slightly larger (see below), the fit would not improve appreciably.

In order to get a better fit, we used a three-component model consisting of an approximate "King" model, dominating at the outermost radii, a power law contributing heavily at the midrange radii, and a central point source dominating in the innermost bins. There are six parameters in this model (r_c, Σ_K, α, r_{pow}, Σ_{pow}, and Σ_{pt}); varying all of them at the same time with five values per parameter would mean constructing over 15,000 models per iteration. The time required to do this would be unacceptable. Instead, we varied four parameters per iteration while holding the others fixed. The resulting 625 models per iteration (five values per parameter) could be constructed in a reasonable amount of time. We changed the combination of parameters that we were varying throughout the fitting process.

The final model was reached after 44 iterations, the first seven of which used the compressed image. As was the case for the NGC 1316 fits, the model profiles fell off more steeply than the observed profiles at large radii (greater than 2" in this case), where the field background may be important. We thus included a constant background parameter in our models for the last 19 iterations. The final model had a "King" core radius of 1".65, a power-law index of 1.31, and a power-law core radius of 0".022. The best-fit background was 0.3 counts pixel^{-1}, on the order of the expected theoretical background for this exposure (0.27 counts pixel^{-1}). The χ^2 was 57.3 for 32 degrees of freedom.

The best-fit model and the observed profile are shown in Figure 8*a*; the residuals of the fit are shown in Figure 8*b*. The two innermost bins in the model profile are higher than the observed values. This discrepancy is probably due to saturation of the central pixels of the brightness distribution. With a count rate of 0.156 counts s^{-1} in the central pixel, the detector response becomes nonlinear at a level of up to 30% (Greenfield et al. 1992).

We also attempted to fit the profile with a power-law + point source model, as done for the F480LP image of NGC 1316. In present instance, however, this model does not give an acceptable fit to the data. The best-fit model had $\chi^2 = 656.9$ for 35 degrees of freedom, indicating a much poorer fit than the "King" + power-law + point source model.

B3. NGC 1316 F175W

The radial surface brightness profile of the UV observation of NGC 1316 appears to be composed of a strong central spike and a more extended distribution, which dominates at larger radii. In addition, the background makes a strong contribution, causing the profile to become virtually flat at distance more than 2" from the center (Fig. 4). The effect of the high background is to make the fitting of the extended component very ambiguous. With this in mind, we compared the models generated for this observation with background-subtracted images. We subtracted two levels of background from the observed image, the theoretical background and the background measured from the area of the image with the lowest emission. When our model produced a profile that fell between those produced by the two levels of background subtraction, we deemed it acceptable. We did not calculate a χ^2 for this model because of the uncertainties in the background level and the synthetic point spread function. In our fit of the power-law plus point source, we fixed the power-law index and core radius at the values determined for the F480 filter observation. The point source and power law normalizations were varied to give the best fit "by eye" (Fig. 11). This introduces the assumption that the power law has no significant color gradient. However, with our data we cannot test this assumption.

B4. DISCUSSION ON GOODNESS OF FITS

The minimum χ^2 values for the NGC 1316 and NGC 3998 F480LP "best fits" are rather high and correspond to formally unacceptable fits ($P \leq 1\%$). This indicates that either the models are not a good representation of the data, or that the errors do not follow a normal distribution. The first possibility is unlikely, since we do not find any systematic trends in the distributions of the fit residuals with radius, and the best-fit models reproduce quite closely the observed brightness profiles (see Figs. 5 and 8). However, if we plot the histograms of these residuals, we find that they do not follow the normal distribution that would be expected if the only source of error were counting statistics. Typically, these distributions (Fig. 14) are wider than Gaussian, giving a larger number of outlier points, and therefore larger χ^2 than expected for a normal distribution. This suggests that there is another error term that we have not considered in our data. As said in § 3.2, we have only considered statistical errors on the surface brightness for our fits. Uncertainties deriving from the flat-fielding of the FOC images are not included, nor is included an error term to take into account the fluctuations of the stellar field, and possible small-scale variations in the extinctions. Stellar fluctuations should not affect the *average* surface brightness distribution, which is what we are studying and should not be included in the error. Variations in the

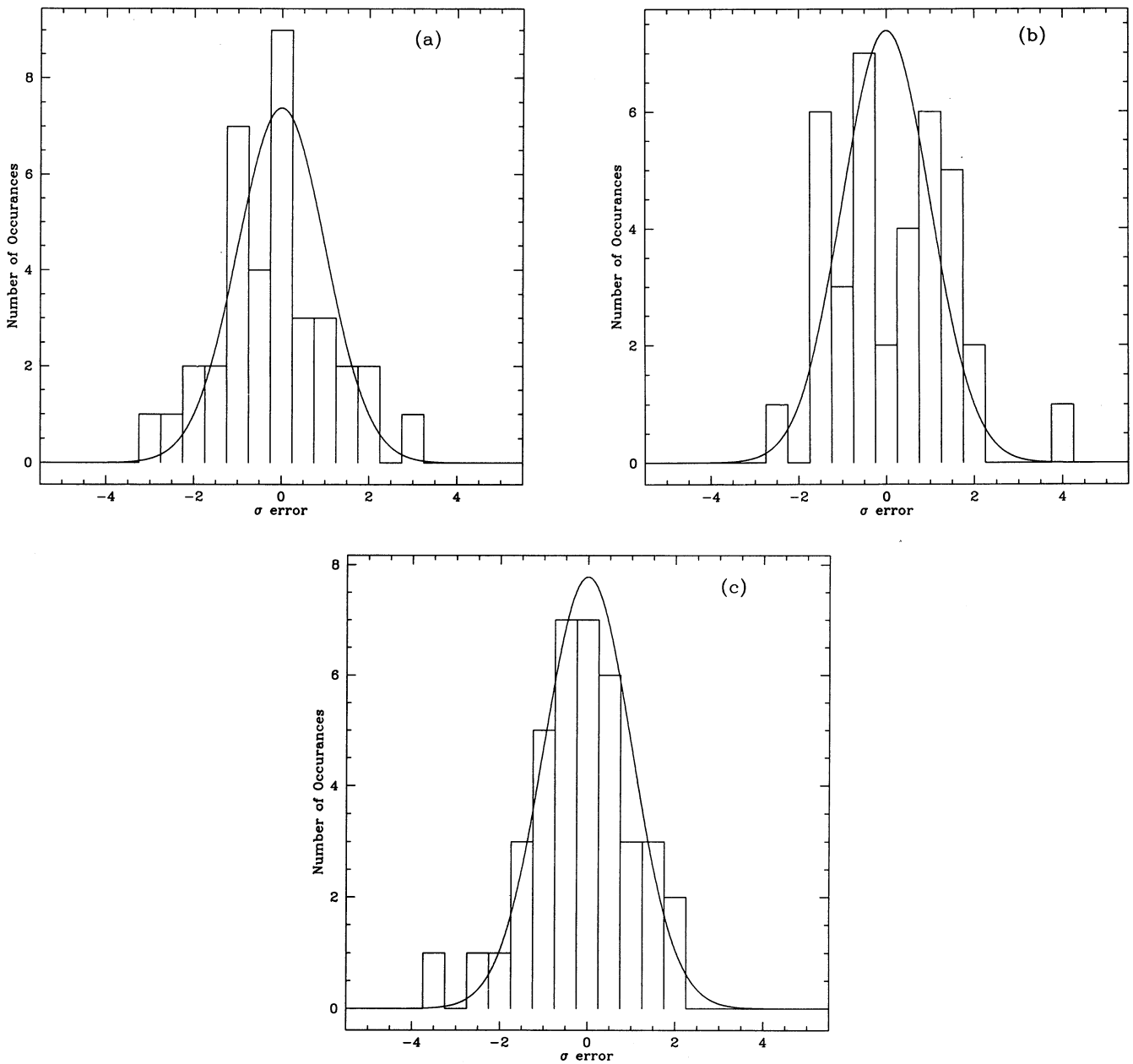

FIG. 14.—Distributions of fit residuals compared with Gaussians. (*a*) NGC 1316 F480LP King + power-law model; (*b*) NGC 1316 F480LP power-law model; (*c*) NGC 3998 F480LP King + power-law + point source model.

extinction may have an effect, depending on their typical angular scale (i.e., if they are on scales larger than the typical annular radius under consideration). Inclusion of these effects would give us smaller χ^2 values.

A different way of estimating the errors is that adopted in STSDAS to use the RMS of the pixel-to-pixel surface brightness variations (§ 3.2). This method takes into account all the microroughness of the surface brightness distribution. However, it clearly overestimates the errors, especially at the outer radii, where the statistical errors are instead relatively small (see Fig. 4). The result is values of χ^2 that are too small. For example, our best-fit power-law model to the F480LP image of NGC 1316 gives a $\chi^2 = 0.562$ for $\nu = 26$ when compared to the surface brightness profile generated by fitting elliptical isophotes to the observed image, where the errors are the RMS of the pixel to pixel surface brightness variations (§ 3.2).

Given that the major uncertainties in our modeling arise from the likely presence of extinction in the central region of NGC 1316 (see § 5) and from the presence of a slightly saturated central point source in NGC 3998, we feel that our present effort is adequate, and we defer further analysis to when *I*-band data with the corrected *HST* optics may be available. For the present, one must remember that while the best-fit parameters are our best representation of the data, the formal uncertainties on these parameters as quoted in Table 4 are likely to be underestimated. If the typical error corresponded to a deviation of $\sim 1.2\ \sigma$, we would obtain formally good best fit χ^2's. In this case, the uncertainties on the fit parameters quoted in Table 4 would correspond approximately to the 68% confidence.

REFERENCES

Avni, Y. 1976, ApJ, 210, 642
Baum, S. A., Heckman, T. M., & Van Bruegel, W. 1992, ApJ, 389, 208
Binney, J., & Tremaine, S. 1987, Galactic Dynamics (Princeton: Princeton Univ. Press), 234
Crane, P., et al. 1993, AJ, 106, 1371
Czerny, B., & Elvis, M. 1987, ApJ, 321, 305
Dressler, A. 1980, ApJ, 40, L11
Dressler, A., & Richstone, D. O. 1990, ApJ, 348, 120
Fabian, A. C., & Canizares, C. R. 1988, Nature, 333, 829
Fabbiano, G. 1988, ApJ, 325, 544
Fabbiano, G., Gioia, I. M., & Trinchieri, G. 1989, ApJ, 347, 127
Fabbiano, G., Kim, D.-W., & Trinchieri, G. 1992, ApJS, 80, 531
Fabbiano, G., Miller, L., Trinchieri, G., Longair, M., & Elvis, M. 1984, ApJ, 277, 115
Filippenko, A. V., & Sargent, W. L. W. 1989, ApJ, 342 L11
Ford, H. C., Dahari, O., Jacoby, G. H., Crane, P. C., & Ciardullo, R. 1986, ApJ, 311, L7
Geldzahler, B. J., & Fomalont, E. B. 1984, AJ, 89, 1650
Greenfield, P., et al. 1991, in Space Astronomical Telescopes and Instruments, ed. P. Y. Bely & J. B. Breckinridge (Bellingham: SPIE), 16
Greenfield, P., et al. 1992, Faint Object Camera Science Verification Report (Baltimore: STScI)
Heckman, T. M., Balick, B., & Crane, P. C. 1980, A&AS, 40, 295
Keel, W. C. 1983, ApJ, 269, 466
Kim, D.-W., Fabbiano, G., & Trinchieri, G. 1992, ApJS, 80, 645
King, I. R. 1978, ApJ, 222, 1
Knapp, G. R., Gunn, J. E., & Wynn-Williams, C. G. 1992, ApJ, 399, 76
Kormendy, J. 1988a, ApJ, 325, 128
———. 1988b, ApJ, 335, 40
———. 1992, ApJ, 338, L9
Lauer, T. R. 1985, ApJS, 57, 473
Lauer, T. R., et al. 1991, ApJ, 369, L41
———. 1992a, AJ, 103, 703
———. 1992b, AJ, 104, 552
Lucy, L. B. 1974, AJ, 79, 745
Paresce, F., ed. 1992, Hubble Space Telescope Faint Object Camera Instrument Handbook (Baltimore: STScI)
Press, W. H., Flannery, B. P., Teukolsky, S. A., & Vetterling, W. T. 1988, Numerical Recipes (Cambridge: Cambridge Univ. Press)
Rees, M. 1984, ARA&A, 22, 471
Reichert, G. A., Branduardi-Raymont, G., Filippenko, A. V., Mason, K. O., Puchnarewicz, E. M., & Wu, C.-C. 1992, ApJ, 387, 536
Richardson, W. H. 1972, J. Opt. Soc. Am., 62, 52
Richstone, D., Bower, G., & Dressler, A. 1990, ApJ, 353, 118
Sargent, W. L. W., Young, P. T., Boksenberg, A., Shortridge, K., Lynds, C. R., & Hartwick, F. D. A. 1978, ApJ, 221, 731
Schweizer, F. 1979, ApJ, 233, 23
———. 1981, ApJ, 246, 722
Willner, S. P., Elvis, M., Fabbiano, G., Lawrence, A., & Ward, M. J. 1985, ApJ, 299, 443
Young, P. J., Westphal, J. A., Kristian, J., Wilson, C. P., & Landauer, F. P. 1978, ApJ, 221, 721